Phase change material-based nano-cavity as an efficient optical modulator

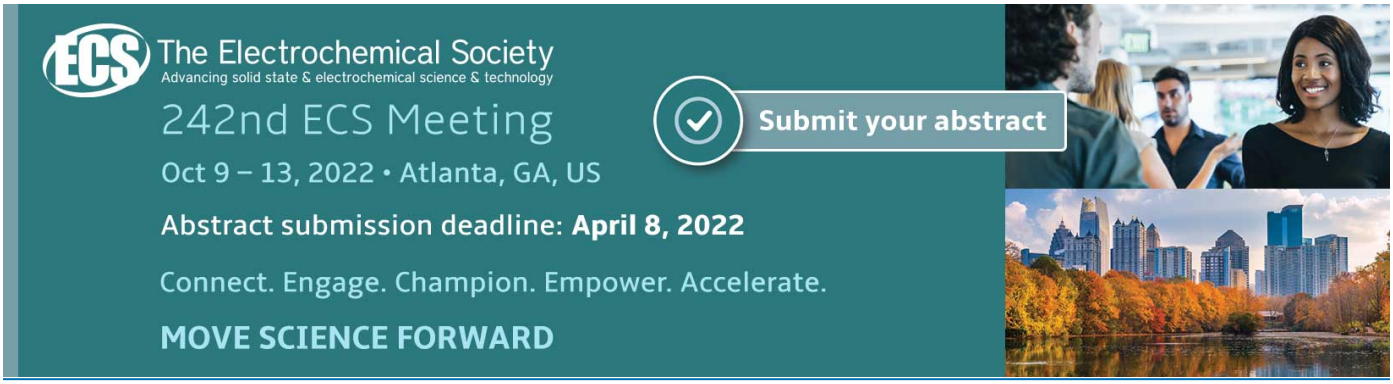

IOP Publishing Nanotechnology
Nanotechnology 32 (2021) 095207 (8pp) https://doi.org/10.1088/1361-6528/abcb7a

Phase change material-based nano-cavity as an efficient optical modulator

Sandeep Kumar Chamoli[1,2], Gopal Verma[1], Subhash C Singh[1,3,*] and Chunlei Guo[3,*]

[1] The Guo China–US Photonics Laboratory, State Key Laboratory of Applied Optics, Changchun Institute of Optics, Fine Mechanics and Physics, Chinese Academy of Sciences, Changchun 130033, People's Republic of China
[2] University of Chinese Academy of Science, Beijing 100039, People's Republic of China
[3] The Institute of Optics, University of Rochester, Rochester, NY 14627, United States of America

E-mail: ssingh49@ur.rochester.edu and guo@optics.rochester.edu

Received 8 August 2020, revised 27 October 2020
Accepted for publication 13 November 2020
Published 8 December 2020

Abstract

Structural phase transition induced by temperature or voltage in phase change materials has been used for many tunable photonic applications. Exploiting reversible and sub-ns fast switching in antimony trisulfide (Sb_2S_3) from amorphous (Amp) to crystalline (Cry), we introduced a reflection modulator based on metal–dielectric–metal structure. The proposed design exhibits tunable, perfect, and multi-band absorption from visible to the near-infrared region. The reflection response of the system shows >99% absorption of light at normal incidence. The maximum achievable modulation efficiency with a narrow line width is ~98%. Interestingly, the designed cavity supports critical resonance in an ultrathin ($\sim\lambda/15$) Sb_2S_3 film with perfect, broadband, and tunable absorption. Finally, we proposed a novel hybrid cavity design formed of Cry and Amp Sb_2S_3 thin films side-by-side to realize an optical modulator via relative motion between the incident light beam and cavity. The proposed lithographic free structure can be also used for filtering, optical switching, ultrathin photo-detection, solar energy harvesting, and other energy applications.

Keywords: nano-photonics, phase change materials, thin film Fabry–Perot (FP) cavity, optical modulator

(Some figures may appear in colour only in the online journal)

1. Introduction

Optical modulators (OMs) are an important component of modern photonic integrated circuits. The OMs have wide applications in both digital and analog communications such as telecommunication, on chip photonics, optical imaging, and frequency comb generation [1–4]. The emergence of handheld optical devices such as optical computers, miniaturized spectrometers, optical sensors etc further increase the importance of OMs [5–7]. Recently, different switching mechanism were reported to design and fabricate reflection/transmission based tunable OMs [8–11]. For example; a graphene/SiO_2 multilayer structure was proposed to design a reflective OM utilizing strong dependence of graphene conductivity on external bias voltage [8]. A metal–dielectric–metal (MDM) plasmonic waveguide was designed as an absorption switch in which the cavity is filled with a material with tunable absorption [9].

Recently, one dimensional nanograting and nanorods and two-dimensional nanostructures, made of phase change materials (PCM), were used as reflective electro-optic modulator. In these OMs, the refractive index of the nanostructures was actively controlled through reversible Amp to Cry phase transition to control the characteristics of reflected/transmitted optical signal [10–12]. Unlike liquid crystals, PCMs provide high optical contrast between the two states with significantly fast switching speed of few nanoseconds. Moreover, the non-volatile characteristic of PCMs increased

* Authors to whom any correspondence should be addressed.

their applications in emerging field of integrated photonics [13, 14]. However, most of the previously designed PCM-based OMs have sub-nanoscale structures or antennas relying on multi-step, tedious, and complex processes for their fabrication that limits scaled production of high efficiency OMs at a low cost [10–12]. Germanium–antimony–tellurium and vanadium dioxide (VO_2) are commonly used PCMs having optical response limited to the infrared spectral region due to high losses in visible [15]. However, high quality factor (Q-factor) tunable nanophotonics devices in the visible demands PCM material having less absorption in the visible and near infrared region (NIR). Sb_2S_3 is a suitable PCM for visible photonics due to its large band gap, high index contrast, strong stability at room temperature and far less lossy than commonly used PCMs in the visible and NIR [15]. Many planar heterostructure designs combining Sb_2S_3 with metals such as Al, Ag and Au have been proposed previously for solar cell application [15, 16]. However integration of noble metals with Sb_2S_3 is still challenging due to diffusion. To prevent diffusion between the metal and PCMs, a 5 nm thick diffusion layer of Si_3N_4 is proposed [15]. Joy *et al* performed a detail experimental analysis on the electrical properties of different metals (Al, Ag, Sb, Sn) with Sb_2S_3 film and their fabrication [17].

Considering above limitations, in this paper, we numerically introduce a thermally/optically tunable MDM-based optical reflective modulator. The tunable phase transition in the dielectric layer of the MDM cavity, made of Sb_2S_3, can actively control its refractive index to build a strong Fabry–Perot (FP) cavity. The reflection response is also sensitive to the incidence angle and polarization of the light. A cavity allow perfect, selective as well as broad band absorptions for the Amp phase of PCM, while close to perfect reflection for its Cry phase to perform optical modulation operations for both s and p polarizations. The modulation in intensity of the reflected light from the designed cavity upon phase transition is as high as ∼98%, even in the case of ultrathin $\lambda/15$ (∼40 nm) cavity. Moreover, the presence of FP resonance in an ultrathin Sb_2S_3 film can also be used for the realization of an ultrathin polarization rotator. We have also realized that the critical coupling condition for FP resonance in ultrathin film demands material with high refractive index. The proposed tunable FP cavity may have many other applications, beyond reflective OM, such as photo detector, color filter, optical sensors, spectroscopy, and photovoltaic.

2. Results and discussions

The schematic of the proposed MDM reflection modulator is shown in figure 1. The structure has three layers on a glass substrate: (a) the bottom layer is silver (Ag) with thickness H, (b) the sandwiched middle layer is Sb_2S_3 with a thickness of h, and (c) the top layer is Ag with thickness of t. Ag is chosen due to having low absorption in the visible. Transfer matrix method is used for all the simulation work using a commercial package (Lumerical Inc.). The refractive index data for Ag and Sb_2S_3 have been taken from [15, 18]. The light in the wavelength range of 400–1000 nm propagates in the downward Z-direction to illuminate the structure. The optimized thickness for top and bottom Ag layers are: $t = 15$ nm and $H = 100$ nm (thick enough to suppress the transmission of light).

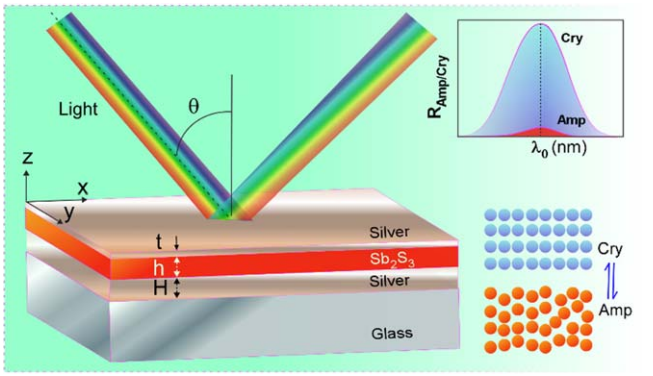

Figure 1. Schematic of proposed optical reflection modulator.

Figure 2(a) represents the refractive index (n) and the extinction coefficient (k) for the Amp and Cry phase of Sb_2S_3 as a function of wavelength, and corresponding spectral changes in n and k due to the phase transition (see figure 2(b)). The Cry phase of Sb_2S_3 exhibits higher refractive index than Amp phase, attaining a max difference of $\Delta n \sim 1$ at 614 nm. The imaginary part decreases with wavelength and reaches to zero at 605 nm for Amp and 721 nm for Cry phase. The resulting high index contrast in Sb_2S_3 can offer high degree of tunability in the proposed MDM-based OM. Phase transition in Sb_2S_3 from Cry to Amp or Amp to Cry phase takes place in 70 ns resulting in ∼7.14 MHz of switching speed or modulation frequency [15]. This attribute of Sb_2S_3 makes it suitable for high speed reprogrammable photonics applications.

The FP interference is the governing mechanism in the MDM structure cavity to explain a selective and broad band absorption. At resonance, the electric field is strongly confined into the PCM dielectric layer as a result of constructive interference between incoming and reflected light. The thickness of Sb_2S_3 has great impact on the resonance condition of the cavity as given by: $2nh = (m + 1/2)\ \lambda_0$, where n is refractive index of cavity, m is the order of mode and λ_0 is the resonance wavelength. According to resonance condition on increasing or decreasing the value of h, the number of modes m supported in the cavity can be increased or decreased. Apart from h the cavity index n also has significant influence on the resonance condition. Therefore, for any material with given h and n, the resonance condition is fixed that imposes limitation on the dynamic nature of MDM cavity i.e. most of the FP cavities are passive components. However, PCM based MDM cavity, where refractive index of PCM can be changed through opto-thermal or electro-thermal effect, can be employed to overcome the limitation and offers tunability in the resonance condition due to high index contrast PCM. The MDM based FP cavity can be used as an active photonic component using PCM as the dielectric layer.

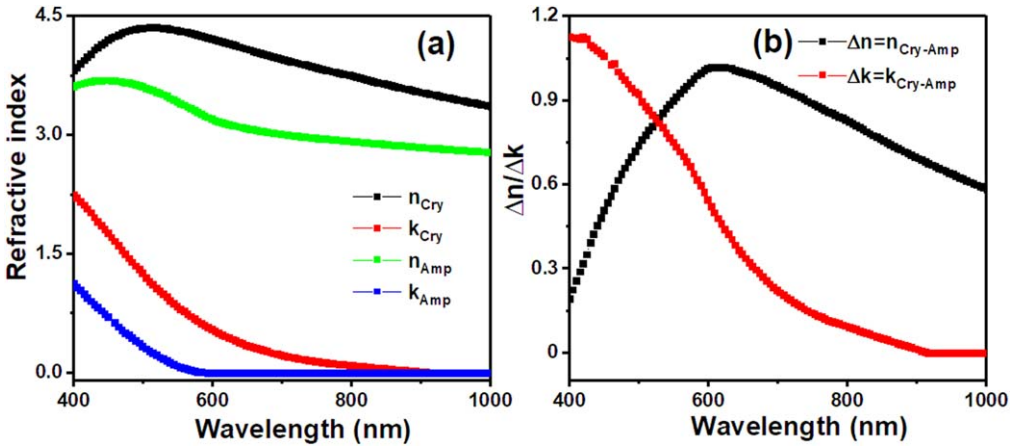

Figure 2. (a) Real and imaginary components of the complex refractive index of Sb_2S_3 between the crystalline (Cry) and amorphous (Amp) phases. (b) Difference of real (Δn) and imaginary part (Δk).

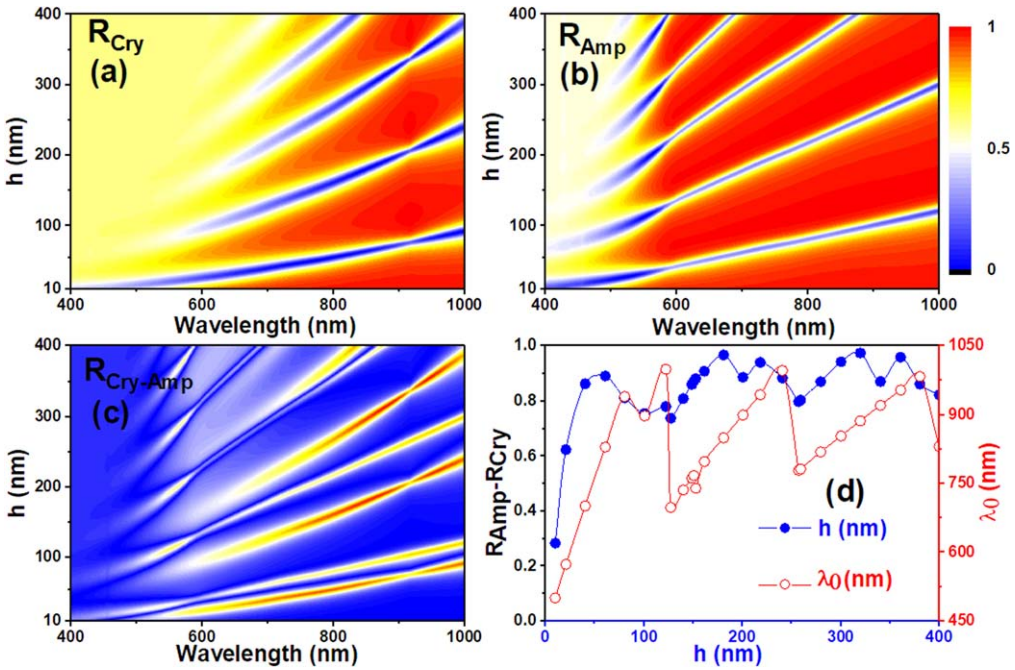

Figure 3. Reflection as a function of Sb_2S_3 thickness (h) and wavelength for S-polarized light for normal incidence (a) Cry phase (b) Amp phase (c) reflection difference between Cry and Amp. (d) Maximum reflection and its corresponding λ_0 and h.

Figures 3(a) and (b) demonstrate the contour plots for spectral reflection as a function of Sb_2S_3 thickness at normal incidence for Cry and Amp phase, respectively. On increasing h from 10 to 400 nm, higher order resonance peaks starts appearing. The number of modes supported in the cavity follows the resonance condition. Even at an ultrathin width of h, the resonance appears in both phases and increase in the h value correspondingly changes the resonance condition

Figure 3(c) presents the change in the reflection due to phase change from Cry to Amp. From the result, it is evident that depending on the wavelength of interest, one can wisely choose the value for h to achieve maximum change in the phase induced reflection ($\Delta R = R_{Amp} - R_{Cry}$) to maximize the modulation coefficient. Figure 3(d) demonstrates variation in the ΔR (the blue curve) and λ_0 (the red curve) with h for normal incidence. Therefore, one can choose the value of h for the wavelength of interest to attain maximum modulation in the reflection. To understand the physical mechanism behind the resonance, we calculated the absorption responses for Ag film on a glass substrate (Ag/glass), 300 nm thick Sb_2S_3 film on the (Ag/glass) substrate and finally Ag–Sb_2S_3–Ag cavity (figures 4(a) and (b)) for Amp and Cry phases of Sb_2S_3. We noticed a negligible absorption from Ag/glass that remained constant with increase in the Ag thickness. For 300 nm thick Sb_2S_3 film on the (Ag/glass) substrate; the absorbance in the Cry phase is higher than the absorption in Amp phase and attains maximum value at ~713 nm. The absorption spectrum of Sb_2S_3 film at Ag/glass substrate shows absorbance according to the Bear–Lambert law upto 605 and 721 nm for Amp and Cry phase, respectively. However, after this wavelength absorption is due to interference between incident and reflected light in the cavity.

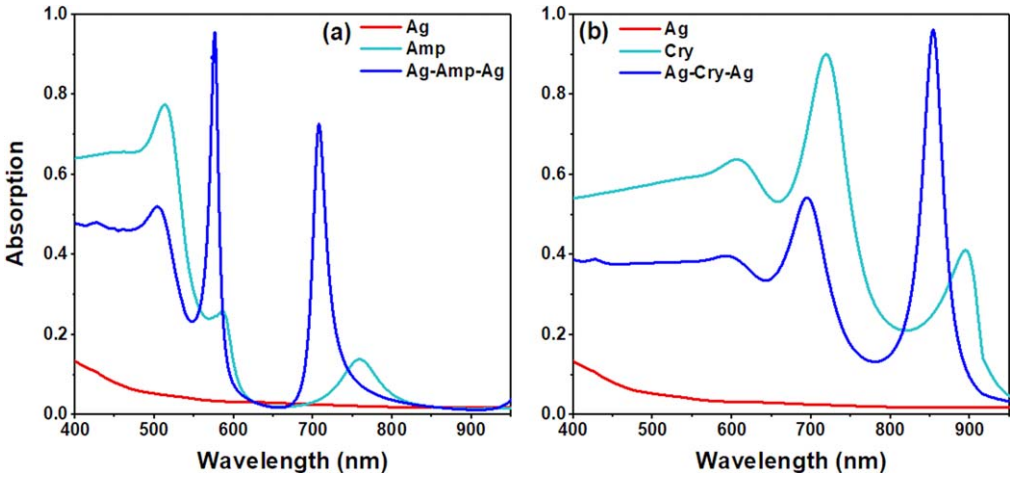

Figure 4. Absorption response from Ag (100 nm), Sb_2S_3 (300 nm)/Ag (100 nm) and Ag (15 nm)–Sb_2S_3 (300 nm)–Ag (100 nm) for (a) Amp phase (b) Cry phase.

In the interference region Sb_2S_3 (Amp)/Ag/glass system acts as a selective mirror after 800 nm. With the addition of top Ag layer, an obvious sharp FP resonance appeared in both phases that confirms FP type resonance in the Ag–Sb_2S_3–Ag cavity (blue colour in figure 4).

Figures 5(a)–(d) represents contour plots for the spectral reflection as a function of incidence angle from Ag–Sb_2S_3–Ag system with 300 nm thick Sb_2S_3 layer. Strong resonance peaks with narrow bandwidth are observed for both polarization and phases due to the formation of strong FP cavity. As expected, the polarization effect is not observed for incident angles <10 degrees in Amp as well as Cry phases, however it is clearly seen in both phases for the larger (>10 degree) incident angles. Figures 5(a) and (b) show reflection corresponding to Cry Sb_2S_3 in MDM cavity for S and P polarized light, respectively. For the S polarized light, only one absorption band centred at ∼850 nm with bandwidth of ∼40 nm is observed where the absorbance decreases with increase in the incident angle and gets completely vanished at ∼75 degree. For P-polarized light, the absorption for ∼850 nm band is strong for all incidence angles from 0 to 90 degree (figure 5(b)). With Cry to Amp phase transition in Sb_2S_3, the reflection response changes significantly as shown in figures 5(c), (d). Three new narrow absorption bands are observed while the band at ∼850 nm completely disappeared. The bandwidths for 573 nm and 703 nm absorption bands are ∼6 nm and ∼38 nm, respectively. At resonance, the reflection is quenched by destructive interference, while strong absorption occurs due to multiple reflection inside the cavity. It is also feasible to broaden the optical absorption by further optimization of top Ag film thickness [19].

Similarly, figures 5(e)–(h) represents the spectral reflection at different incident angles for an ultrathin (35 nm) Sb_2S_3 sandwiched layer. In Amp phase, a strong absorption band centred at $\lambda_0 = 550$ nm with bandwidth ∼100 nm is observed for both polarizations (see figures 5(e), (f)). Upon phase transition to Cry phase the absorption band shows a red shift and broadening for both polarization (see figures 5(g), (h)). The broadband absorption nature of the designed cavity may find useful applications in solar cells and broadband photo-detection. The proposed cavity is dynamic, shows narrow and broad band absorption, and supports critical coupling even for ultrathin cavity by following typical FP resonance. One can wisely select the MDM cavity parameters to tune spectral absorption/reflection in the wavelength of interest for different photonic and optoelectronic applications in visible and NIR spectral regions. Moreover, the modulator shows iridescence free response from normal to 70–80 degrees, due to high index of Sb_2S_3 (see figure 5). This type of design retains all their optical properties even after deposition on rough surfaces [20–22].

The spatial and spectral distribution of electric field intensity profiles in the thick ($h = 300$ nm) and thin ($h = 35$ nm) MDM cavities are shown figure 6 for Cry ($E_{S\text{-}Cry}$) and Amp phase ($E_{S\text{-}Amp}$) using S-polarized light at normal incidence. Electric field is mainly distributed or confined in the middle layer with narrow band and high enhancement at resonance wavelength. Two noticeable field distribution windows can be seen: (i) a window less than 550 and 750 nm in Amp and Cry, which is following a Beer–Lambert region (B. L. region) (ii) after 550 and 750 nm interference regions in which light can completely pass the absorbing media and reflect back from the bottom Ag layer (Inference region). At resonance the electric field is strongly confined into the Sb_3S_3 layer as a result of constructive interference between incoming and reflected light from bottom Ag layer in the interference region or after B. L. region. The spectral field distribution calculated along the thickness of the MDM cavity and shows field enhancement at the resonance wavelength. A clear FP resonance can be seen corresponding to modes presented in figures 5(a), (c) and (e), (g). The modes can be actively switched with the phase transition. For example: the modes at 573 and 713 nm observed in the Amp are not present in the Cry phase (see figures 6(a) and (b)). Due to broadening of the absorption peaks, the intensity in the Cry phase is weaker over the Amp phase. The results show the switchable or tunable nature of proposed MDM-FP cavity and

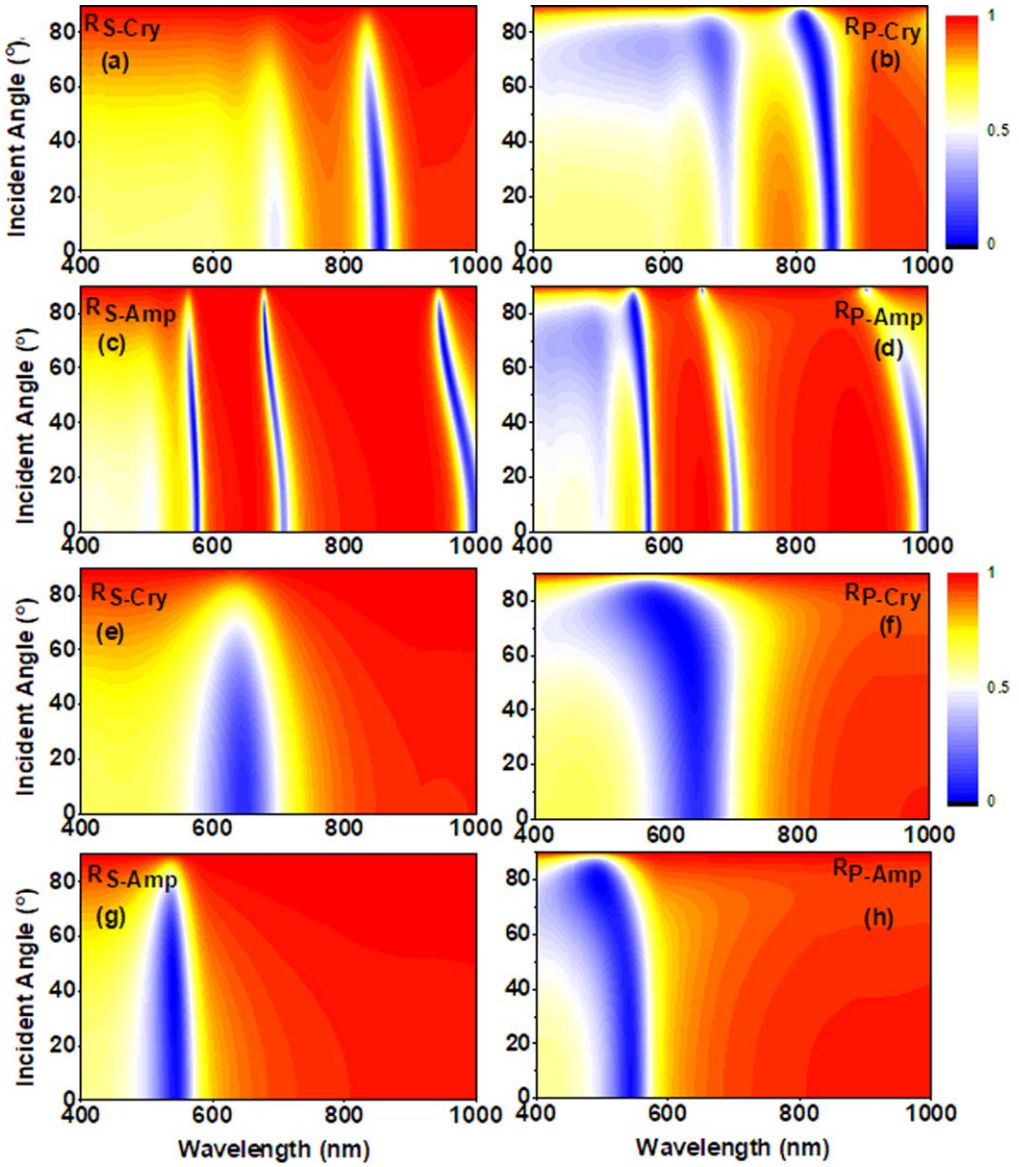

Figure 5. Reflection as a function of incident angle and wavelength in Amp and Cry phase, for $h = 300$ nm (a) S-polarized light—Cry (b) P-polarized light—Cry (c) S-polarized light—Amp (d) P-polarized light—Amp. and for $h = 35$ nm (e) S-polarized light—Cry (f) P-polarized light—Cry (g) S-polarized light—Amp (h) P-polarized light—Amp. $t = 15$ nm and $H = 100$ nm.

motivation to implement it as a reflection switch or modulator.

Furthermore, we introduce a novel hybrid cavity made of rectangular shaped Cry and Amp phases of Sb_2S_3 film side-by-side as shown in figure 7(a). The reflection response for a broadband light beam from (i) Amp and (ii) Cry phase is shown in figure 7(b). However realization of such a design can be challenging but selective heating in the cavity can be achieved by following the strategies discussed in the [23]. Bilayer and tri-layer structures have been proposed using some local heating elements in it. A conventional 'mush-room' shape memory device was accomplished by designing a programmable pulse with varying its amplitude or slope of trailing edge [24, 25]. It was demonstrated that this way one can introduce the selective temperature profile to change the phase of materials selectively [23–25]. Additionally, In a broader aspect one can use any dielectric combination in the same fashion such as TiO_2 and SiO_2 for many application such as linear variable colour filtering application [26].

This type of hybrid cavity can be easily fabricated via deposition of SiO_2/TiO_2 films through a 3D printed or laser etched masks. One can first deposit 'left dielectric- say SiO_2' on Ag film through one half of the rectangular/square slit keeping other half close. Later, other half can be open to deposit 'right dielectric-say TiO_2' while covering the already deposited 'SiO_2'. The advantage of this design is (i) its smaller footprint (minimum size two-times of the light beam) and (ii) higher frequency of modulation. The proposed hybrid cavity can be mounted on a high frequency mechanical oscillator or vibrator to switch position of the beam between two phases. In this scheme the period of modulation is the time required to completely move the light beam from/to Cry phase to/from Amp phase which depends on the diameter of the light beam and frequency of the mechanical oscillator.

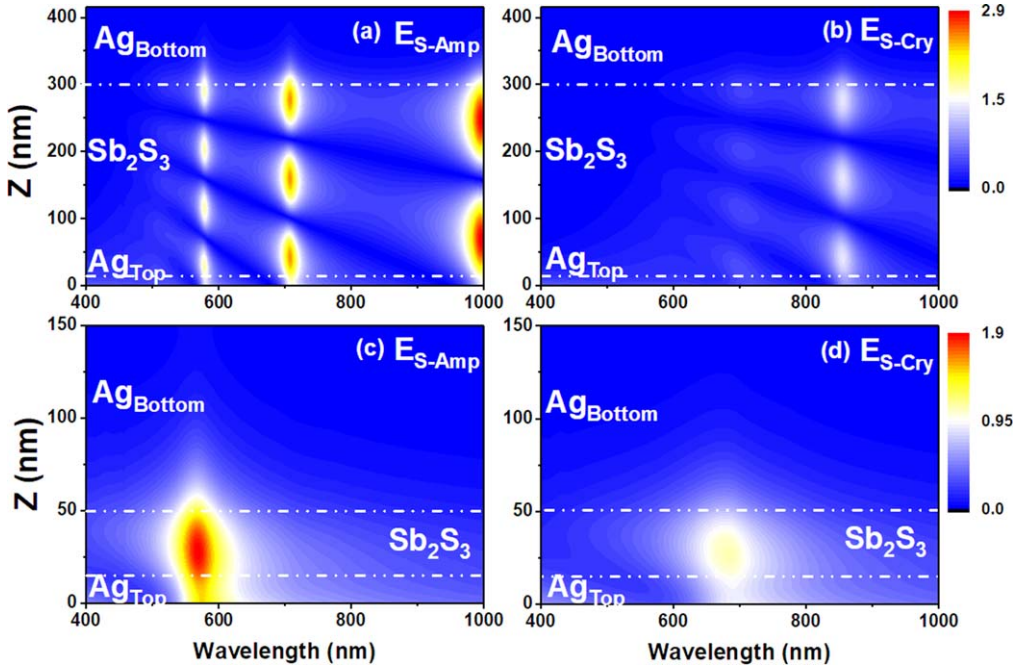

Figure 6. Electric field distribution at normal incidence for s polarized light (a) Amp and (b) Cry phase for $h = 300$, (c) Amp and (d) Cry phase for $h = 35$ nm. $t = 15$ nm and $H = 100$ nm.

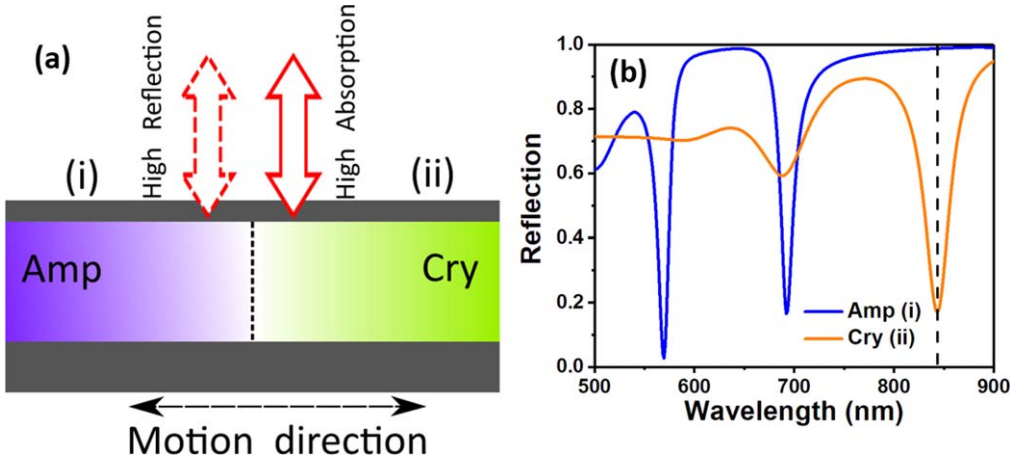

Figure 7. (a) Schematic of proposed novel rectangular shaped Cry and Amp phase Sb_2S_3 cavity. (b) Reflection verses wavelength from the location (i) and (ii). Thickness of cavity = 300 nm. $t = 15$ nm and $H = 100$ nm.

The frequency or switching speed of the modulator could be equal to the frequency of oscillator. For example: employing 1 MHz of oscillator to oscillate the hybrid cavity, the period, amplitude and frequency of the modulated signal would be 1 μs, 1 MHz, and $[R(\lambda)_{\mathrm{Cry}} - R(\lambda)_{\mathrm{Amp}}]\, I(\lambda)$, respectively. Here $R(\lambda)$ and $I(\lambda)$ are reflectance for Cry (Amp) phase and intensity of incident light at the wavelength of operation. The modulator or beam needs to be translate by the length of the diameter of beam. Utilization of the interfacial region of 'Cry' and 'Amp' blocks, the switching period can be reduced by shrinking the diameter of light beam and increasing relative motion between the light beam and modulator.

Finally, the resonance condition in ultrathin film of complex refractive index $(n + ik)$ has been investigated and shown in figures 8(a), (b). We calculated the reflectivity ($\lambda_0 = 573$ and 713 nm) as a function of n and k from a film of thickness 40 nm (see the inset of figures 8(a), (b)). The reflectivity is zero at $3.4 + 0.1i$ and $3.93 + 0.2i$, which corresponds to $\sim\lambda_0/4n$ (quarter wave). Furthermore, these points are correspond to the (n, k) values of Amp and Cry at 573 nm and 713 nm respectively. This demonstrates the switching between maximum absorption points between the two phases. This also indicates that critical coupling condition i.e. a perfect or near perfect absorption in ultrathin lossy symmetric FP demands a high index material. These nanocavities confine light in a very small volume and can be very useful component for compact integrated photonics circuits particularly for cavity quantum electrodynamics, nonlinear optics, sensor and optomechanics and laser with low threshold. So, confinement of the light below the fundamental limit of

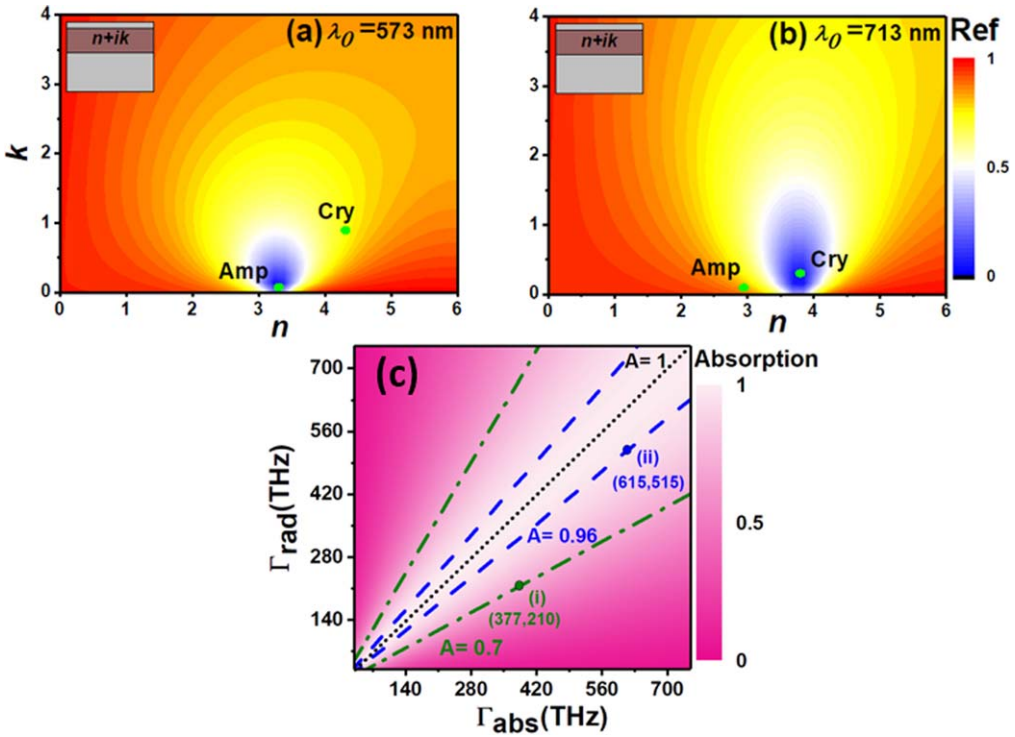

Figure 8. Reflectivity as a function of n and k for a $h = 40$ nm thick film with complex index $(n + ik)$ for (a) 573 nm and (b) 713 nm at normal incident and (c) effect of radiative and absorption rate on the resonant absorption.

diffraction is possible in ultrathin cavity which is the fundamental limit in the conventional dielectric micro-cavities, such as whispering gallery resonators and photonic crystal cavities [27]. Additionally, according to Coupled-mode theory, the critical coupling condition can be achieved once the radiative (Γ_{rad}) and absorptive (Γ_{abs}) decay rates are equal i.e. $\Gamma_{rad} = \Gamma_{abs}$ [28–30] and given by the following expressions [30]:

$$A(\omega) = 1 - \left| r_p + \frac{\Gamma_{rad} e^{i\varphi}}{i(\omega - \omega_0) + (\Gamma_{rad} + \Gamma_{abs})/2} \right|^2, \quad (1)$$

where r_p is background reflection, ω_0 is resonant wavelength and φ is the associated phase with resonant modes. Equation (1) can further reduce to equation (2) in the limit of $r_p \to -1$ and $\varphi \to 0$ [30]:

$$A(\omega) = \frac{\Gamma_{rad}\Gamma_{abs}}{(\omega - \omega_0)^2 + \left(\frac{\Gamma_{rad} + \Gamma_{abs}}{2}\right)^2}. \quad (2)$$

At critical coupling i.e. $\Gamma_{rad} = \Gamma_{abs}$, $A(\omega) = 1$ and absorption peak reaches upto 100% at resonance. The width of peak depends on its quality factor can be calculated as $Q = \frac{\omega_0}{\Delta\omega}$, where $\Delta\omega$ is the full width at half maxima and also $Q = \frac{\omega_0}{\Gamma_{rad} + \Gamma_{abs}}$ according to coupled mode theory. Figure 8(c) represents absorption as a function of Γ_{rad} and Γ_{abs} decay rates. Black dotted line corresponds to $A = 1$ i.e. $\Gamma_{rad} = \Gamma_{abs}$. Green and blue dashed lines are representing $A = 0.7$ and 0.96 respectively. The decay rate ratio of are $\Gamma_{abs} = 1.8\ \Gamma_{rad}$ and $\Gamma_{abs} = 1.19\ \Gamma_{rad}$ at point (i) and (ii) (see inset of figure 8(c)). The points (i) and (ii) also show decay rate correspond to the absorption results present in figures 9(a) and (b) for Amp and Cry, respectively.

Phase shift $\Delta\Psi$ at critical coupling point always expected to be abrupt i.e. $\Delta\Psi$ either 0 or π which is known as phase singularity. It has great applications in label free optical bio sensing [31, 32]. The proposed MDM cavity also demonstrates a tuneable and abrupt phase shift upon reflection. The spectral phase shift ($\Delta\Psi$) in the reflected light and corresponding reflectance from Amp (see figure 9(a)) and Cry (see figure 8(b)) phases for $h = 40$ nm thick Sb_2S_3 film are presented. In Cry stack maximum absorption ~99.15% and $\Delta\Psi \sim \pi$ can be noted at $\lambda_0 = 691$ nm. However, in Amp stack maximum absorption with $\Delta\Psi = 0$ is at $\lambda_0 = 573$ nm. Moreover, as $\Delta\Psi$ upon reflection from the cavity is commonly different for s and p component of the electric field, therefore changing the polarization state. For instance, a relative phase shift of $\pm\pi$ rotates linear polarization and the transformation between linear and circular polarizations requires phase shift of $\pm\pi/2$.

Finally, one of the key parameters for any OM, a 3 dB bandwidth (Δf) and quality factor (Q) have been calculated using expressions given below in equations (3) and (4):

$$\Delta f = f_{lower} - f_{upper} \quad (3)$$

$$Q = f_0 / \Delta f, \quad (4)$$

where f_0 is the central frequency and f_{lower} and f_{upper} are correspond to lower and upper cut-off frequency point where modulation decrease to 70.7% of maximum. So, the calculated (Δf, Q) corresponds to Amp and Cry in figures 9(a) and (b) are (4.36 × 106 Hz, 12.29) and (4.6 × 106 Hz, 9.33).

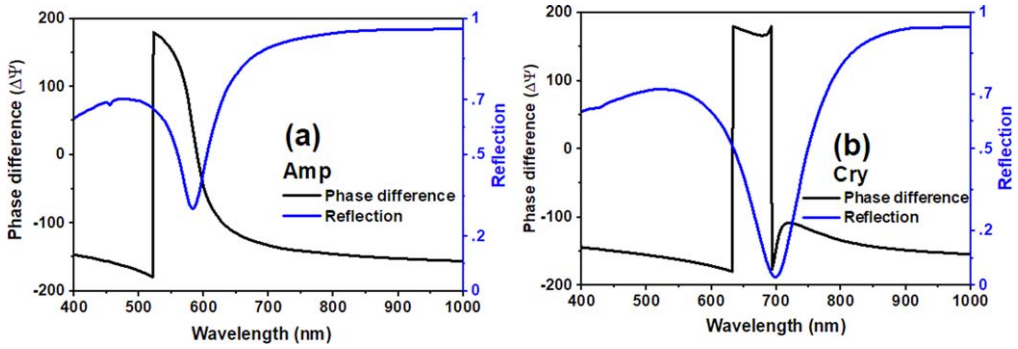

Figure 9. Reflection and phase difference ($\Delta\Psi$) as a function of wavelength for $h = 40$ nm of (a) Amp and (b) Cry phase.

3. Conclusion

In summary, we numerically demonstrated a PCM based reflective type OM with ~98% modulation efficiency. The phase transition in cavity provides a solution to dynamically control reflectance of the incident signal in a broad angle of incidence for wavelength ranging from visible to near infrared. The cavity reflection response has been investigated as a function of Sb_2S_3 thickness with its importance to fix the resonance condition. Depending upon the thickness, the cavity can support multiple absorption bands. The minimum thickness of the PCM layer that can supports critical coupling of light is $\sim\lambda/15$. We have also demonstrated that the critical coupling requires a dielectric with high refractive index. At the end hybrid cavity made of rectangular shaped Cry and Amp phase of Sb_2S_3 has been proposed, in which both the phases can act together and increase the switching speed manyfold. The proposed reflection modulator is easy to fabricate, low cost and can be mass produced at low cost for many other applications, beyond OM, such as spectral filtering for solar cells, smart windows, optical sensors, sensing, fluorescence control, photodetection and so on.

Acknowledgments

S K C gratefully acknowledges his sponsorship by 'CAS-TWAS Presidential's Fellowship for international doctorate students'.

Funding

National Science Foundation (NSF) (1263236, 0968895, 1102301); The 863 Program (2013AA014402)

ORCID iDs

Sandeep Kumar Chamoli https://orcid.org/0000-0002-8297-4081
Gopal Verma https://orcid.org/0000-0003-3246-4646
Subhash C Singh https://orcid.org/0000-0002-8139-1124
Chunlei Guo https://orcid.org/0000-0001-8525-6301

References

[1] Romagnoli M *et al* 2018 *Nat. Rev. Mater.* **3** 392
[2] Atabaki A H *et al* 2018 *Nature* **556** 354
[3] Zhang M *et al* 2019 *Nature* **568** 373
[4] Fan K, Suen J Y and Padilla W J 2017 *Opt. Express* **25** 25318
[5] Chamoli S K, Singh S and Guo C 2020 *IEEE Sens. J.* **20** 4628
[6] Chamoli S K, Singh S and Guo C 2020 *IEEE Sens. Lett.* **4** 1–5
[7] Chamoli S K, Singh S and Guo C 2020 *Plasmonics* **15** 1339
[8] Pianelli A, Kowerdziej R, Dudek M, Sielezin K, Olifierczuk M and Parka J 2020 *Opt. Express* **28** 6708
[9] Wang X, Kuwahara M, Awazu K, Fons P, Tominaga J and Ohki Y 2009 *Opt. Express* **17** 16947–56
[10] Min C *et al* 2009 *Opt. Express* **17** 10757
[11] Ahmadivand A, Gerislioglu B and Pala N 2017 *Phys. Chem.* C **121** 19966
[12] Ding F, Yang Y and Bozhevolnyi S I 2019 *Adv. Opt. Mater.* **7** 1801709
[13] Zhang Y *et al* 2019 *Nat. Commun.* **10** 4279
[14] Wuttig M, Bhaskaran H and Taubner T 2017 *Nat. Photon.* **11** 465
[15] Dong W *et al* 2018 *Adv. Funct. Mater.* **29** 1806181
[16] Kondrotas R, Chen C and Tang J 2018 *Joule* **2** 857
[17] George J and Radhakrishana M K 1980 *Int. J. Electron.* **49** 397
[18] Palik E D 1985 *Handbook of Optical Constants of Solids* (New York: Academic)
[19] Li Z, Butun S and Aydin K 2015 *ACS Photonics* **2** 183
[20] ElKabbash M, Ilker E, Letsou T, Hoffman N, Yaney A, Hinczewski M and Strangi G 2017 *Opt. Lett.* **42** 3598
[21] Schlich F F and Spolenak R 2013 *Appl. Phys. Lett.* **103** 213112
[22] Kats M A and Capasso F 2014 *Appl. Phys. Lett.* **105** 131108
[23] Wong H S P *et al* 2010 *Proc. IEEE* **98** 2201
[24] Rao F, Song Z, Zhong M, Wu L, Feng G, Liu B, Feng S and Chen B 2007 *Jpn. J. Appl. Phys.* **46** 25
[25] Lai Y F, Feng J, Qiao B W, Cai Y F, Lin Y Y, Tang T A, Cai B C and Chen B 2006 *Appl. Phys.* A **84** 21
[26] Ji P, Park C-S, Gao S, Lee S-S and Choi D-Y 2017 *Opt. Express* **25** 2153
[27] Lu Q, Shu F-J and Zou C-L 2013 Dielectric bow-tie nanocavity *Opt. Lett.* **38** 5311–4
[28] Fan S, Suh W and Joannopoulos J D 2003 *J. Opt. Soc. Am.* A **20** 569
[29] Guo Y and Fan S 2016 *Opt. Express* **24** 29896–907
[30] Krishnan A, O'Gorman A B and Povinelli M L 2020 *J. Opt.* **22** 094002
[31] Kravets V *et al* 2013 *Nat. Mater.* **12** 304
[32] Sreekanth K V, Han S and Singh R 2018 *Adv. Mater.* **30** 1706696